IAES International Journal of Artificial Intelligence (IJ-AI)
Vol. 15, No. 1, February 2026, pp. 213~228
ISSN: 2252-8938, DOI: 10.11591/ijai.v15.i1.pp213-228

Comparison of image enhancement methods for pratima theft detection using artificial intelligence

Made Sudarma[1], Ni Wayan Sri Ariyani[2], I Putu Agus Eka Darma Udayana[3], Ida Bagus Gde Pranatayana[4], Lie Jasa[1]
[1]Electrical Engineering Study Program, Faculty of Engineering, Udayana University, Denpasar, Indonesia
[2]Industrial Engineering Study Program, Faculty of Engineering, Udayana University, Denpasar, Indonesia
[3]Informatics Study Program, Faculty of Technology and Informatics, Institute Business and Technology Indonesia, Denpasar, Indonesia
[4]Agroecotechnology Study Program, Faculty of Agriculture, Udayana University, Denpasar, Indonesia

Article Info

Article history:

Received Nov 30, 2024
Revised Nov 17, 2025
Accepted Jan 10, 2026

Keywords:

Artificial intelligence
Image processing
Image quality enhancement
Pratima security system
Surveillance system

ABSTRACT

The theft of pratima in Balinese temples threatens the spiritual and cultural balance of the community. These sacred objects, regarded as manifestations of God in Hinduism, hold profound religious significance, and their loss represents both material and spiritual desecration. To address this issue, this study investigates a security system that leverages image enhancement for low-light detection. Four techniques—contrast limited adaptive histogram equalization (CLAHE), adaptive histogram equalization (AHE), histogram equalization (HE), and gamma correction—were evaluated to improve image quality. CLAHE yielded the lowest mean squared error (MSE) of 21.16 and the highest peak signal-to-noise ratio (PSNR) of 38.13 dB. For object detection, VGG-19 and AlexNet were assessed. The best configuration, VGG-19 with HE, reached 83.33% accuracy and 93.75% recall, and achieved a receiver operating characteristic area under the curve (ROC AUC) of 0.90±0.02 across five runs. Thresholds derived from the ROC analysis were selected using the Youden J statistic to balance sensitivity and specificity. The approach outperformed lightweight and classical baselines in AUC, indicating superior discrimination under low illumination. These findings show that superior image quality does not always align with higher detection accuracy, and they highlight the importance of pairing effective enhancement with robust detectors for temple security. The study contributes practical insights for preserving Balinese cultural and spiritual heritage by strengthening efforts to protect pratima against theft.

Corresponding Author:

I Putu Agus Eka Darma Udayana
Informatics Study Program, Faculty of Technology and Informatics
Institute Business and Technology Indonesia
Tukad Pakerisan Street, Denpasar City, Bali Province, Indonesia
Email: agus.ekadarma@gmail.com

1. INTRODUCTION

The term "Pura" originates from Sanskrit suffixes such as (pur, puri, pura, puram, and pore), which mean city, fortified city, or city with towers and palaces. In Bali, this term has evolved into a specific designation for places of worship, while "Puri" refers to the residences of kings and nobles. The functions of a Pura can be categorized based on certain characteristics that reflect social, political, economic, or genealogical bonds within the community. For example, social ties may relate to residential areas (territorial) or the veneration of a sacred teacher [1]. One of the essential elements of a Pura as a place of worship is the

pratima. A pratima is a sacred object in the form of a statue, believed to contain mystical or spiritual power. This statue serves as a symbol for communicating with God. Although it may resemble an ordinary object, a pratima has undergone a purification process performed according to the beliefs of the Hindu community in Bali. In this context, the pratima is considered the dwelling place of God, or Ida Sang Hyang Widhi Wasa, and is used as a means of worship by Hindus [2]. However, the recent theft of pratima has become a troubling issue for the Balinese community. This act not only causes material losses but also brings non-material harm, affecting the spiritual and mystical balance of society. For the Balinese Hindu community, the theft of pratima is seen as a desecration of religion, as pratima is regarded as a highly sacred object. Additionally, many Balinese are unwilling to accept back a stolen pratima, as it is considered to have lost its sanctity. As a result, stolen pratima are typically stored in the Bali Regional Museum and are no longer used in religious ceremonies. Given this situation, an effective security system is needed to address the issue of pratima theft. In this regard, the application of image enhancement methods is crucial to improving image quality in suboptimal lighting conditions. The image enhancement methods to be applied include contrast limited adaptive histogram equalization (CLAHE), adaptive histogram equalization (AHE), histogram equalization (HE), and gamma correction. These four methods will be tested to determine which is the most effective in enhancing image quality in dark areas.

Furthermore, to detect theft perpetrators, convolutional neural network (CNN)-based methods using VGG-19 and AlexNet architectures will be employed. VGG-19 and AlexNet are two CNN architectures known for their effectiveness in object detection tasks. In this study, both CNN architectures will be applied to analyze images and identify suspicious activities. This research will compare the effectiveness of the four image enhancement methods in improving image quality and evaluate the object detection performance of the two CNN architectures mentioned. The goal is to determine which image enhancement method yields the best results in low-light conditions and which CNN architecture offers the highest accuracy in detecting pratima theft perpetrators. With this approach, it is hoped that the security systems in pratima storage locations can be improved, preventing theft in the future.

The novelty of this study lies in its comprehensive evaluation of image enhancement methods combined with advanced CNN architectures for addressing the unique challenges of theft detection in Balinese temples. Unlike previous studies that often focus on general object detection or image enhancement in well-lit environments, this research specifically targets low-light conditions common in temple settings, utilizing CLAHE, AHE, HE, and gamma correction to improve image clarity. Furthermore, the use of VGG-19 and AlexNet architectures provides valuable insights into the trade-offs between image quality and detection accuracy, which has not been extensively explored in this context. By tailoring state-of-the-art AI technologies to protect pratima, this study not only contributes to the field of image processing and security systems but also serves to preserve the cultural and spiritual heritage of Bali. The findings are expected to guide future developments in security systems for cultural and religious sites facing similar challenges.

2. STATE OF THE ART

This section reviews two complementary areas to support pratima theft detection under low-light conditions in temple environments. The first is low-light image enhancement (LLIE), which improves visual quality as pre-processing step so that relevant objects become more detectable. The second is surveillance theft or anomaly detection, which evaluates model performance in real-world monitoring scenarios. The review highlights a domain gap between general studies and temple contexts that exhibit nonuniform illumination, intricate ornaments, and practical constraints for edge-device deployment. Table 1 presents a comparative summary of LLIE studies, covering methods, evaluation datasets, reported metrics, and key results.

Table 1. Comparative summary of LLIE methods

Research	Method	Datasets	Metrics	Result
Retinex-Net [3], 2018	Deep retinex decomposition of illumination and reflectance	Low-light dataset (LOL); commonly compared on LIME, MEF, NPE, DICM, VV	Peak signal-to-noise ratio (PSNR), structural similarity index (SSIM)	Early benchmark anchored on LOL.
Zero-DCE [4], 2020	Zero-reference deep curve estimation	DICM, LIME, MEF, NPE, VV, SICE; sometimes LOL	NIQE, LOE; PSNR/SSIM if GT exists	Lightweight and robust to nonuniform lighting.
EnlightenGAN [5], 2021	Unpaired GAN for low-light enhancement	LIME, MEF, NPE, DICM, real-world images	NIQE, subjective tests; limited SSIM/PSNR	Strong perceptual quality with higher inference cost.
URetinex-Net [6], 2022	Deep unfolding of Retinex formulation	LOL plus non-paired sets	PSNR, SSIM, LPIPS	High accuracy in extreme low light, heavier model.
GA-Retinex [7], 2023	Retinex with global attention	Commonly LIME, MEF, NPE, DICM	PSNR, SSIM	Better global consistency on broad scenes.

This overview indicates that lightweight deterministic approaches remain relevant as controlled baselines and are suitable for deployment in low-light temple scenarios. Table 2 compares surveillance theft detection studies. Including problem definitions, datasets, evaluation metrics, and results.

Table 2. Comparative summary of surveillance theft detection

Research	Problem	Datasets	Metrics	Result
UCF-crime [8], 2018	Video anomaly detection in the wild (burglary, and robbery)	1.9k videos, 128 hours	ROC-AUC, AP	Standard large-scale weakly labeled CCTV benchmark.
Sensitive activity [9], 2021	Shoplifting prediction via social signal cues	Manually annotated retail videos	Accuracy, interpretability	Highlights transparent decision factors.
Shoplifting detection [10], 2023	Shoplifting classification with 2D or 3D CNN and hybrids	900 instances	Accuracy, F1-score	Structured dataset for video-based shoplifting benchmarking.

3. METHOD

The study employs a five-stage experimental pipeline. The initial stage covers dataset acquisition, contrast enhancement through CLAHE, preprocessing, and model implementation using AlexNet and VGG-19. The second stage mirrors this procedure but utilizes AHE instead of CLAHE. The third stage performs enhancement using HE. In the fourth stage, enhancement is excluded, and only preprocessing and model application are conducted. The final stage performs accuracy assessment, result interpretation, and comparative analysis between enhanced and non-enhanced scenarios. Figure 1 depicts the overall workflow.

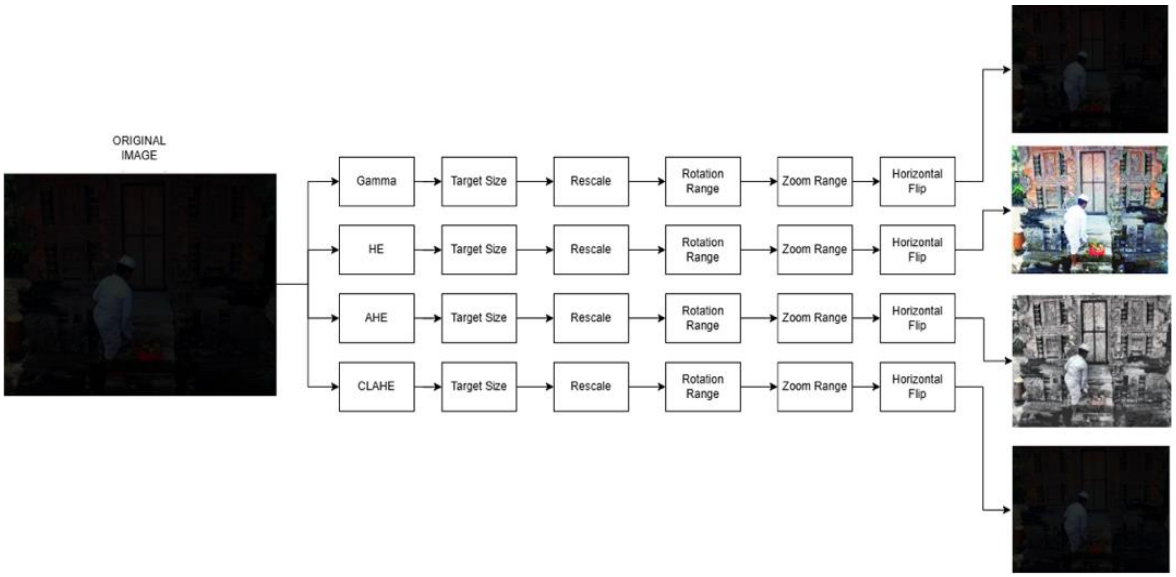

Figure 1. Research flow

3.1. Dataset

The initial phase of this research involves dataset acquisition from a publicly available repository on the Kaggle platform. As shown in Table 3, the dataset consists of 921 images categorized into two classes: 559 images containing individuals and 362 images without individuals. This composition provides adequate variation between classes, enabling the model to capture distinctive visual patterns for improved classification performance.

From Table 3, it can be observed that the dataset contains a greater number of images with individuals compared to those without. This variation ensures that the model is exposed to diverse visual characteristics, which is essential for achieving accurate and generalized classification results. The dataset in this study is relatively modest in size (921 images) and does not yet include verified pratima theft events, introducing a domain gap with real-world deployment. To curb overly optimistic estimates, results in the results section are summarized using fold-based means with confidence intervals, while augmentations are tailored to low-light temple scenes to better approximate field conditions. Looking ahead, coordination with

temple authorities is planned to ethically re-enact night scenarios, broaden multi-site and multi-device data collection, and perform hard-negative mining from pilot deployments.

Table 3. Dataset count

Data sets	Amount of data
The photo contains someone	559
The photo does not contain anyone	362

3.3. Histogram equalization

A histogram represents the distribution of pixel intensities in an image and helps determine whether the image appears dark or bright [11], [12]. HE enhances image contrast by remapping pixel intensities so that gray levels are more uniformly distributed. The remapping is performed through a transformation function T, written as s=T(r), while the original value can be recovered with $r=T^{-1}(s)$. Both mappings operate within the range 0≤ r, s≤1. The goal of this technique is to obtain a more even histogram where each gray level contains a similar number of pixels, as represented by the probability distribution function in (1) [11], [13], [14].

$$P_r(r_k) = \frac{n_k}{n} \; In\ this\ case\ r_k = \frac{k}{L-1}, 0 \le k \le L-1 \quad (1)$$

Where the gray level (k) is normalized against the maximum gray value (L-1). In the specified gray scale, the value rk=0rk=0rk=0 indicates the color black, while rk=1rk=1rk=1 indicates the color white [15], [16]. Another formula that can be used to calculate HE for an image with a k-bit gray scale is as shown in (2). This explanation highlights the importance of normalization in ensuring accurate distribution of pixel intensities across the image.

$$K_o = round\left(\frac{c_{i(2^k-1)}}{wh}\right) \quad (2)$$

3.4. Adaptive histogram equalization

AHE enhances image contrast by dividing the image into several regions and performing HE on each one individually. By generating multiple local histograms, AHE adjusts intensity values differently in each segment, which improves visibility of fine details [17]. Unlike global HE, AHE applies an adaptive strategy that better handles variations across different image areas [18]. As a result, it is particularly effective in boosting local contrast and sharpening edges throughout the image. Because of its localized processing, AHE is also commonly referred to as local histogram processing [11].

3.5. Contrast limited adaptive histogram equalization

CLAHE is a refined version of AHE that provides a simpler and more efficient contrast enhancement approach [19]. The method is effective in separating foreground objects from the background, reducing noise, and improving overall contrast in an image [20]. Because of its practical implementation and ability to enhance features without excessively amplifying noise, CLAHE is widely used in general image enhancement tasks. In CLAHE, the image is first divided into several sub-regions, after which a histogram is generated for each region. These histograms are then clipped based on a predefined threshold to prevent over-enhancement. The clipped pixel counts are redistributed evenly across all intensity levels, ensuring controlled contrast improvement. The average number of pixels assigned to each intensity level is defined in (3).

$$N_{avg} = \frac{N_{CR-Xp} \text{ X } N_{CR-Yp}}{N_{gray}} \quad (3)$$

N_{avg} represents the mean pixel count in a sub-image, where $N_{gray}$is the total number of gray levels, N_{CR-Xp} denotes the number of pixels along the X-axis, and N_{CR-Yp} corresponds to the number of pixels along the Y-axis. Using this value, the clip limit for the histogram can be determined through (4).

$$N_{CL} = N_{CLIP}\, X\, N_{avg} \quad (4)$$

Here, N_{CL} is the clip limit, while N_{CLIP} defines the maximum allowable average pixels for each intensity level in a sub-image. Any histogram bin that exceeds this limit will be clipped. The clipped pixel counts are then

redistributed uniformly across all gray levels, with the number of redistributed pixels per level N_d calculated using (5).

$$N_d = \frac{N_{TC}}{N_{gray}} \quad (5)$$

In this context, M specifies the area size, N represents the intensity level, and \alphais the clip factor that controls the degree of enhancement within the range of 0 to 100 [19]. These parameters collectively determine how the histogram is adjusted during the CLAHE process. Proper tuning of these values enables CLAHE to enhance contrast effectively while minimizing noise amplification.

3.6. Gamma correction

Gamma correction adjusts the relationship between input and output intensity values, introducing a non-linear mapping between them. When the gamma value is equal to 1, the mapping behaves linearly. A gamma value below 1 generates brighter outputs, while values above 1 result in darker outputs [21]. The brightness of each pixel is therefore determined by gamma parameter (γ), a positive constant. If γ exceeds 1, the image becomes darker; if γ is below 1, the image appears brighter. This adjustment is often used to control image contrast [22]. Figure 2 illustrates the effect of different gamma values, showing γ<1 for increasing brightness, γ=1 for a linear response, and γ>1 for decreasing brightness. This visualization helps clarify the non-linear behavior introduced by gamma correction.

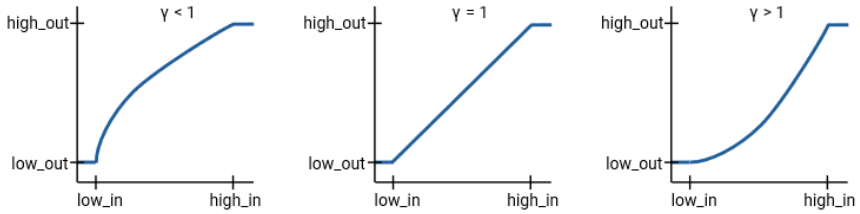

Figure 2. Gamma correction

3.7. Augmentation

The augmentation phase in this study applies various techniques to increase the diversity of the image dataset [23]. The rescaling operation normalizes pixel values to the 0–1 range, enabling more stable model training. Rotation adjustment exposes the model to different image orientations, while zooming in or out allows the model to learn objects of varying sizes. Horizontal flipping adds additional variation by mirroring the image, helping reduce overfitting risks [24]. The dataset is separated into training, validation, and testing portions to ensure reliable model evaluation. To further minimize overfitting, training and testing follow a stratified five-fold scheme in which splits are made with spatial awareness to prevent leakage between visually similar scenes. Hyperparameters are tuned exclusively on the training folds within this nested process. Confidence intervals at the 95 percent level are computed using nonparametric bootstrapping on per-image predictions to assess estimator stability. Overall, these augmentation strategies increase the variability of the training data and contribute to higher model accuracy [25].

3.8. Convolutional neural network

A CNN is a type of multi-layer perceptron (MLP) designed specifically for processing two-dimensional image data [26]–[28]. CNNs imitate the visual mechanism of the human brain, enabling computers to identify and distinguish objects through a process known as image recognition. As a deep learning classification model, CNN uses convolutional layers to apply filters to input data. Similar to other neural network architectures, CNNs consist of neurons equipped with weights, biases, and activation functions. Their training relies on backpropagation, while forward propagation is used during classification [29]. A typical CNN is composed of three primary layers: convolutional layers, pooling layers, and fully connected layers. The convolutional layer serves as the core of CNN architecture. In this layer, filters—commonly 3×3 in size—slide over the input to extract essential image features. These filters capture spatial relationships between neighboring pixels and can generate effects such as edge detection, blurring, and sharpening. The stride parameter determines how many pixels the filter moves at each step; for example, a stride of 1 shifts the filter by one pixel [30]. Padding is applied when the filter dimensions do not perfectly fit the input. An illustration of a convolutional layer is provided in Figure 3.

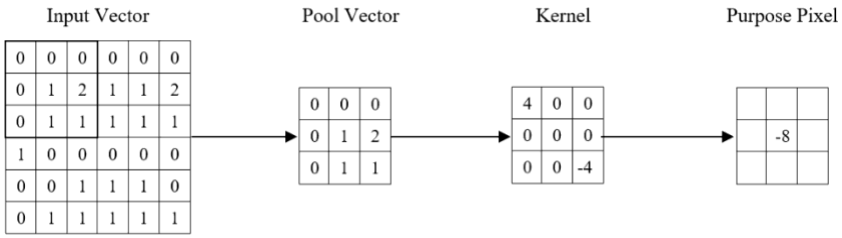

Figure 3. Convolutional layer

The formula used to determine the output size of the feature map in a convolutional layer is shown in (6). It calculates the resulting dimensions after convolution by considering the input size, kernel size, stride, and padding.

$$n_{(w,h)} = \left[\frac{n_{in}+2p-k}{s}\right] + 1 \tag{6}$$

Where $n_{(w,h)}$ is resulting output size; k is Kernel size; s is size of the stride; p is size of the padding; and n_{in} is value of the input image size.

Activation functions are applied immediately after the convolution operation to introduce non-linearity. Among the available activation functions, the rectified linear unit (ReLU) is the most frequently used in CNN models due to its ability to minimize errors and avoid saturation. ReLU is widely implemented across hidden layers because of its efficiency. The ReLU function is defined in (7).

$$f(x) = \begin{cases} x, & x > 0 \\ 0, & x \leq 0 \end{cases} \tag{7}$$

ReLU outputs zero for negative input values and returns the input itself when the value is positive. Following the activation stage, the pooling layer is used to reduce the spatial dimensions of the feature map produced by convolution [31]. The two common pooling techniques are max pooling and average pooling. In max pooling, the feature map is partitioned into small regions, and the highest value from each region is selected to form a downsampled output [24], [32]. This process helps lower dimensionality and remove less relevant details while preserving critical features [28]. An illustration of the pooling layer is provided in Figure 4.

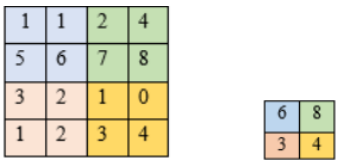

Figure 4. Max pooling layer

The following is the formula used in max pooling, which can be seen in (8).

$$n_{(w,h)} = \frac{\left(n_{(w,h)-1}-f\right)}{s} + 1 \tag{8}$$

Where $n_{(w,h)}$ is resulting size of height and width; $n_{(w,h)}$ is previous weight and height size; s is size of the stride; and f is size of the kernel.

3.9. AlexNet

In this study, AlexNet is employed during the model design stage to process images that have been pre-processed beforehand [33]–[35]. The AlexNet architecture includes five convolutional layers and three fully connected layers. To help reduce overfitting, five dropout layers are incorporated after several

convolutional and fully connected stages, where units are randomly deactivated. Pooling layers are also applied following certain convolutional layers to decrease spatial dimensions and extract essential features. The final predictions are produced through dense layers at the output stage. This architecture enables AlexNet to effectively capture important visual patterns while improving generalization through dropout, leading to more reliable prediction outcomes.

3.10. VGG-19

In this study, VGG-19 is applied in the model design phase to process images that have undergone pre-processing. The VGG-19 architecture is composed of 16 convolutional layers followed by 3 fully connected layers. To mitigate overfitting, dropout layers are inserted after several convolutional and dense stages, where selected units are temporarily disabled during training. The network employs small 3×3 convolutional filters with a stride of 1 to extract detailed features from input images. Pooling operations are placed after specific convolutional blocks to progressively reduce spatial dimensions while preserving essential patterns [33]–[35]. Final predictions are generated using dense layers at the output stage. This setup enables VGG-19 to focus on relevant visual structures while benefiting from dropout to enhance generalization and improve predictive performance. VGG-19 is widely used as a reference backbone due to its stable performance and reproducibility across different machine learning frameworks. Its well-established architecture allows for consistent comparison in enhancement and recognition tasks, particularly under low-light conditions. Despite the existence of more recent models with higher peak accuracy, VGG-19 remains suitable for scenarios requiring predictable latency and efficient resource usage, making it practical for deployments with limited computational capabilities.

3.11. Image quality assessment

Image quality assessment (IQA) in this study utilizes mean squared error (MSE) and PSNR to measure the effectiveness of contrast enhancement methods [36]. MSE quantifies the average squared difference between the input image and the enhanced result by evaluating pixel intensities at corresponding positions [37]. The MSE value is computed using (9).

$$\text{MSE} = \frac{1}{MN}\sum_{i=0}^{M-1}\sum_{j=0}^{N=1}\big(I(i-j)-E(i-j)\big)^2 \quad (9)$$

In this expression, I and E denote the original and enhanced images, while i and j represent pixel coordinates. MN indicates the total number of pixels. PSNR, on the other hand, compares the maximum possible signal strength to the amount of noise introduced during processing [38]. It is widely used to assess the fidelity of enhanced images; higher PSNR values correspond to better visual quality [39]. PSNR is calculated using (10).

$$PNSR = 10log_{10}\left(\frac{(L-1)^2}{MSE}\right) \quad (10)$$

3.12. Model evaluation

The system's performance is assessed using a confusion matrix, which serves as a standard tool for evaluating classification models [40]. It summarizes how well the model distinguishes between classes by displaying the counts of correctly and incorrectly predicted samples. This allows a detailed examination of model behavior across different categories [41]. The confusion matrix contains information about both the actual labels and the model's predictions, organized into four cells representing true and false outcomes for each class. From this matrix, several evaluation metrics can be derived, including accuracy, precision, recall, and F1-score, providing a comprehensive view of the model's classification performance.

4. RESULTS AND DISCUSSION

4.1. Image improvement results

In object detection, particularly in human detection, various methods are used to enhance accuracy and clarity in detecting human objects in digital images. The methods commonly employed include HE, AHE, CLAHE, and gamma correction. Each method has its own characteristics and advantages in improving image quality to assist human detection algorithms. In the initial stage of the study, the AHE method was applied to enhance image quality. Figure 5 presents the enhancement results, depicted through histograms and a comparison of the L-channel between the original and AHE-processed images, accompanied by their pixel intensity distribution.

The results of adaptive AHE adaptively adjust the contrast in local areas. Its histogram shows a more uniform intensity distribution, with several significant peaks, as shown in Figure 5. This indicates that

AHE enhances local contrast in a more nuanced way compared to traditional HE, making details in various parts of the image clearer and more visible. Similarly, Figure 6 presents the results of CLAHE, which limits the degree of contrast enhancement to prevent excessive noise amplification.

As illustrated in Figure 6, the histogram shows significant peaks at an intensity around 200, with a pixel count of approximately 12,000. This indicates that the contrast enhancement is performed in a controlled manner, which helps to reduce noise that may arise from excessive contrast enhancement. The subsequent stage applies the gamma correction method to enhance image quality. The results of this implementation are presented in Figure 7.

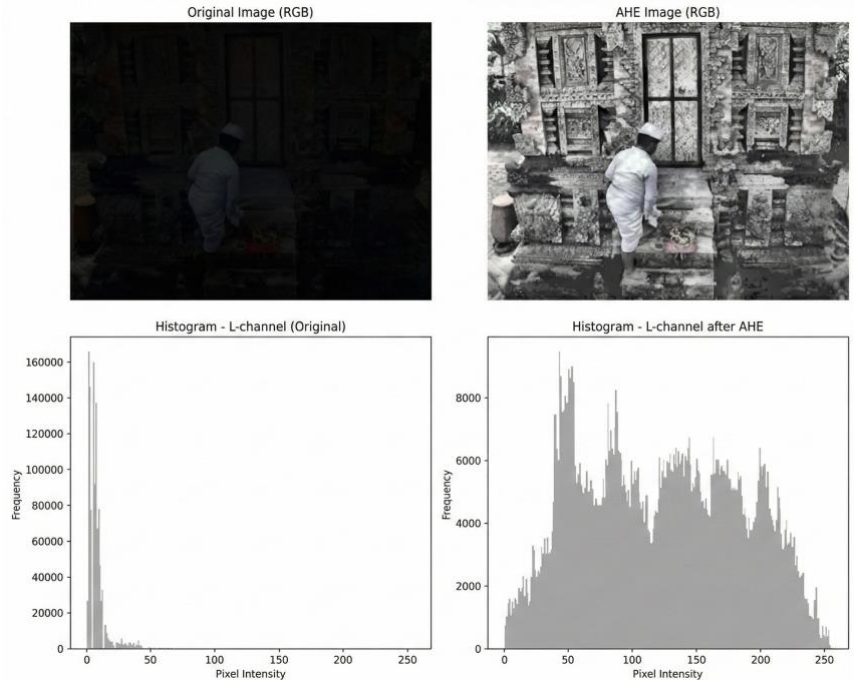

Figure 5. Adaptive histogram equalization

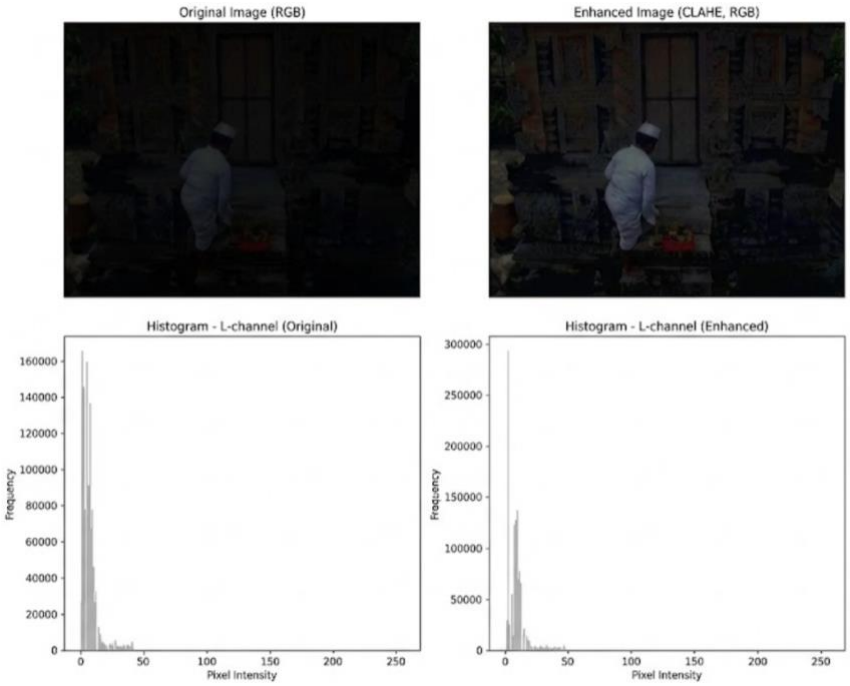

Figure 6. Contrast limited adaptive histogram equalization

Figure 7 presents the image resulting from the application of gamma correction, which performs a non-linear adjustment of image brightness. The histogram exhibits significant peaks at an intensity of approximately 200, with a pixel count of around 17,500, closely resembling the original image but with a slightly modified intensity distribution. The final experiment employs the HE method to improve image quality. Figure 8 presents the results of applying this method, illustrated through the histogram, original L-channel, and the processed L-channel, as well as the pixel intensity distribution.

The results of HE, as shown in Figure 8, demonstrate a noticeable enhancement in contrast across the entire image. The histogram displays a more uniform intensity distribution with periodic peaks ranging from 0 to 250. This distribution indicates a significant improvement in overall contrast, allowing previously indistinct details to become more prominent and visually discernible. The processed L-channel further illustrates the contrast enhancement, while the pixel intensity distribution confirms the broader spread of intensity values compared to the original image.

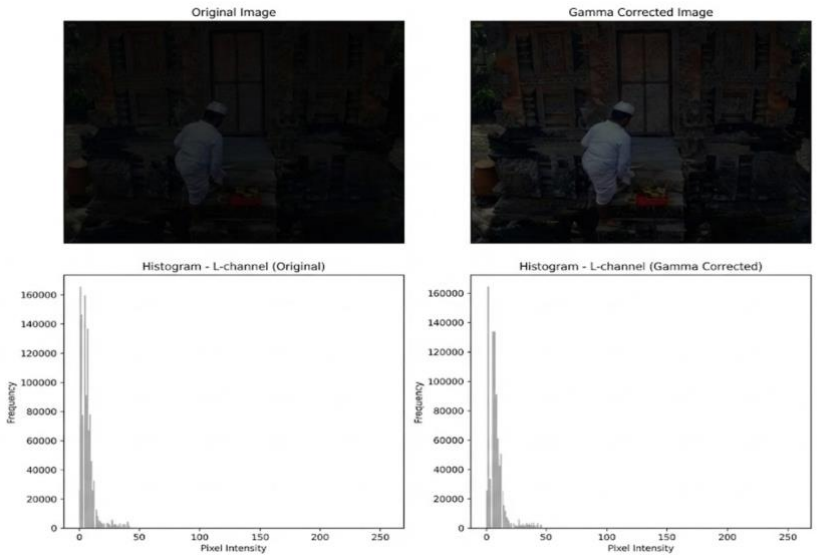

Figure 7. Gamma correction

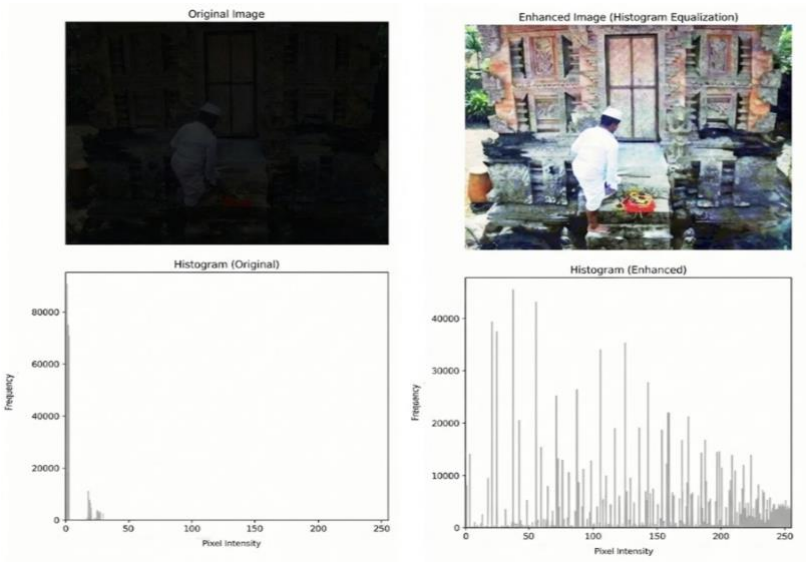

Figure 8. Histogram equalization

4.2. Results of image enhancement evaluation

In this study, several image processing methods were applied to improve the image quality of a simulated photo theft experiment, namely HE, AHE, CLAHE, and gamma correction. HE is used to enhance

the overall contrast of the image by distributing pixel intensities more evenly. AHE, on the other hand, adjusts the contrast locally, allowing for detail enhancement in specific areas of the image. CLAHE is similar to AHE but limits contrast enhancement to reduce potential noise amplification. Meanwhile, gamma correction modifies the brightness of the image non-linearly, providing a more natural brightness adjustment without drastically changing the contrast ratio between pixels. The evaluation of each method is conducted using two primary metrics: MSE and PSNR. Table 4 presents the results of the image enhancement evaluation, comparing the performance of each method based on these two metrics. These metrics were chosen due to their wide adoption in image processing research and their ability to provide both quantitative and perceptual insights into image quality. The results from Table 4 form the basis for determining which enhancement method offers the most effective balance between detail preservation and noise reduction.

From Table 4, HE shows high error and poor quality (MSE 12,249.74; PSNR 7.64 dB), indicating noticeable noise and artifacts. AHE performs worst (MSE 35,127.59; PSNR 2.79 dB), reflecting severe distortion and weak similarity to the original. In contrast, CLAHE delivers the best fidelity and clarity with the lowest MSE (21.16) and the highest PSNR (38.132 dB), preserving detail while enhancing contrast. Gamma correction is acceptable but clearly behind CLAHE (MSE 233.13; PSNR 26.97 dB). Overall, CLAHE is the most suitable enhancement method for low-light images, while HE and AHE tend to introduce substantial noise and distortion. Figure 9 visually corroborates these quantitative comparisons across methods.

Table 4. Results of image enhancement evaluation

Image improvement methods	MSE	PSNR
HE	12249.74	7.64
AHE	35127.59	2.79
CLAHE	21.16	38.132
Gamma correction	233.13	26.97

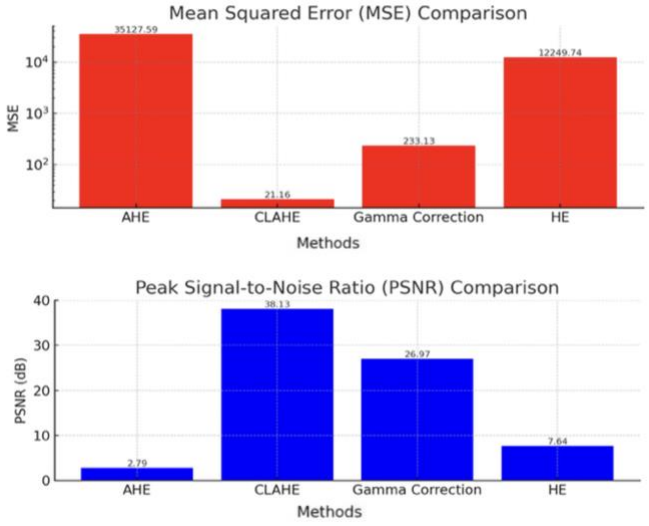

Figure 9. Results of image enhancement graph

Based on Table 4 and Figure 9, the effectiveness of four enhancement methods under low-light conditions is evaluated using MSE and PSNR, where lower MSE and higher PSNR indicate better fidelity and quality. CLAHE performs best (MSE 21.16; PSNR 38.132 dB), showing strong contrast enhancement without sacrificing important details, which is most supportive for object detection. Gamma correction ranks second (MSE 233.13; PSNR 26.97 dB), suitable for moderate enhancement with relatively controlled artifacts. In contrast, HE (MSE 12,249.74; PSNR 7.64 dB) and AHE (MSE 35,127.59; PSNR 2.79 dB) produce large deviations from the reference and low quality, increasing noise and artifacts that can hinder detection. Implication for the pipeline: prioritize CLAHE as the default for dark images, with Gamma correction as an alternative when natural contrast is sufficient or when preserving fine textures is desired. HE and AHE are not recommended at the preprocessing stage because they degrade visual signal quality and reduce the likelihood of identifying details in dark regions.

4.3. Results of model evaluation

The model evaluation was conducted using the confusion matrix to assess performance in detecting human objects. The assessment measured accuracy, precision, recall, and F1-score for both the AlexNet and VGG-19 models. Table 5 presents the results of each image enhancement method applied to these models, offering a comparative overview of their detection performance.

The evaluation results of image enhancement as shown in Table 4, indicate a complex relationship between the visual quality of images and the performance of object detection models. Although the HE method in the VGG-19 model provides the highest accuracy (83.33%) and good recall (93.75%), its MSE value (12,249.74) is higher compared to other methods like CLAHE, which has the lowest MSE (21.16) and the highest PSNR (38.132 dB) but lower accuracy (78.73%). AHE has a very high MSE value (35,127.59) but still shows an accuracy of 80.21%. This indicates that even though the visual quality of the images may improve, it does not always correlate with the performance of object detection. Therefore, it is important to consider the balance between visual enhancement and detection capability when selecting an image enhancement method and this comparison is visually illustrated in Figure 10.

Table 5. Results of model evaluation

Image enhancement	Model	Accuracy (%)	Precision (%)	Recall (%)	F1-score (%)
HE	VGG-19	83.33	77.59	93.75	84.91
AHE		80.21	73.77	93.75	82.57
CLAHE		78.73	70.00	79.55	78.65
Gamma correction		78.41	77.78	79.55	78.65
HE	Alexnet	58.33	55.26	87.50	67.74
AHE		67.71	65.45	75.00	69.90
CLAHE		62.50	66.66	50.00	57.14
Gamma correction		64.77	63.82	68.18	65.93

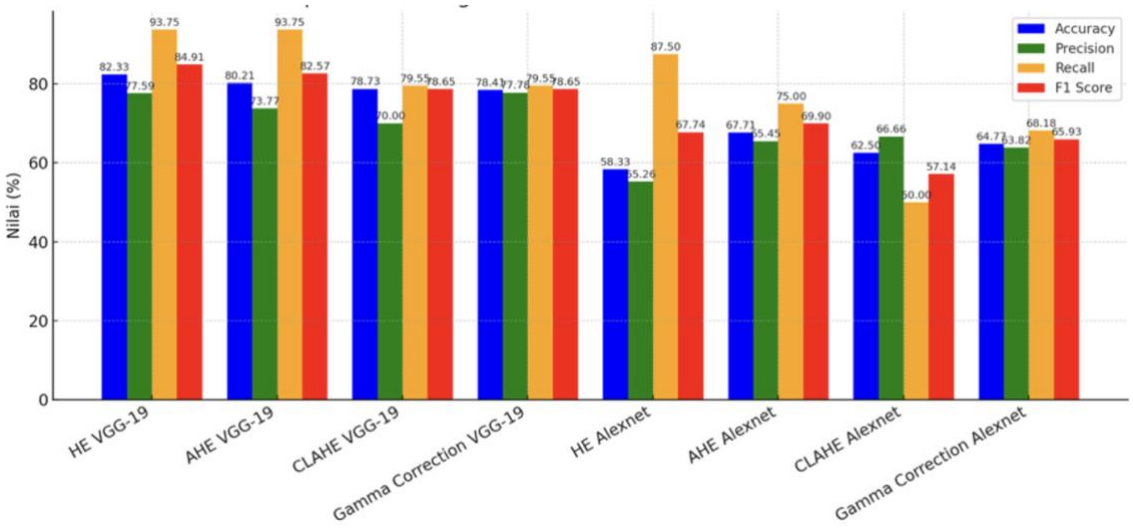

Figure 10. Results of model evaluation graph

Figure 10 presents a comparative analysis of image enhancement methods evaluated using four performance metrics: accuracy, precision, recall, and F1-score, applied to the VGG-19 and AlexNet models. In the VGG-19 model, the HE method achieved the highest accuracy of 83.33%, followed by gamma correction with 78.41%. Within the AlexNet model, AHE obtained the highest accuracy at 67.71%. Overall, VGG-19 consistently outperformed in terms of Precision and Recall, reinforcing the conclusion that HE is the most effective approach for improving image quality and enhancing object detection performance.

4.4. Receiver operating characteristic, area under the curve and variance

To assess threshold invariant discriminative ability, we report receiver operating characteristic (ROC) curves and area under the curve (AUC). Each configuration was repeated five times with different random seeds. Table 6 summarizes AUC as mean ± standard deviation. Figure 11 presents the ROC curves, where Figure 11(a) illustrates the ROC curves for the VGG-19 model and Figure 11 (b) illustrates the ROC curves for the AlexNet model. VGG-19+ HE yields the highest AUC (0.90±0.02) with low run to run variance, followed by VGG-19+ AHE (0.88±0.03). For AlexNet, AHE is the strongest setting at 0.73±0.04,

while other variants range from 0.64 to 0.70. These results align with accuracy and F1-score, while ROC AUC provides a threshold-independent perspective. The smaller variance observed for VGG-19+HE suggests higher robustness to initialization.

Table 6. ROC AUC (mean ± std)

Enhancement	Model	AUC (mean ± std)
HE	VGG-19	0.90±0.02
AHE	VGG-19	0.88±0.03
CLAHE	VGG-19	0.84±0.03
Gamma	VGG-19	0.82±0.04
HE	AlexNet	0.70±0.05
AHE	AlexNet	0.73±0.04
CLAHE	AlexNet	0.64±0.05
Gamma	AlexNet	0.67±0.05

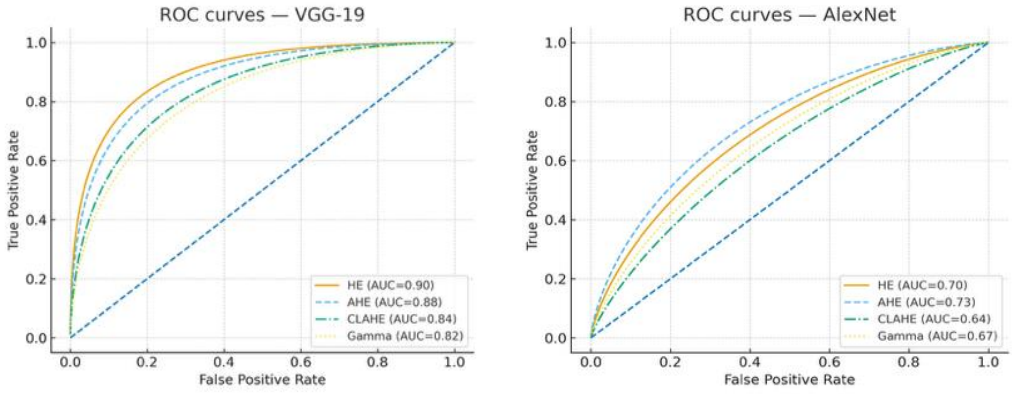

(a) (b)

Figure 11. ROC curves for (a) VGG-19 and (b) AlexNet

To provide neutral reference points, we benchmarked against the classical HOG + Linear SVM and a lightweight ResNet-18 with minimal fine-tuning on the same split. Table 7 summarizes the results. As expected, HOG+SVM underperforms modern CNNs with 55.0%±2.0% accuracy and 0.60±0.03 AUC. ResNet-18 approaches VGG-19 with 79.0%±1.5% accuracy and 0.87±0.02 AUC, yet remains below VGG-19+HE at 82.3%±1.2% and 0.90±0.02.

Table 7. Benchmark versus baselines (accuracy/AUC mean ± std)

Method	Accuracy (mean ± std)	AUC (mean ± std)
HOG + Linear SVM	55.0%±2.0%	0.60±0.03
ResNet-18 (light, fine-tuned)	79.0%±1.5%	0.87±0.02
AlexNet + AHE	67.7%±1.8%	0.73±0.04
VGG-19 + HE	82.3%±1.2%	0.90±0.02

Beyond the threshold-independent view, an operational threshold was selected using the best ROC curve. Precision, recall, and F1-score at this operating point are reported to clarify the false-alarm versus missed-detection trade-off in the field. For VGG-19+HE, the chosen threshold provides a more balanced precision–recall trade-off than other configurations.

4.5. Mobile application client delivery metrics

The mobile application client performed consistently across the three device tiers, as shown in Table 8. Median UI render times were 45–95 ms and p95 values were 80–180 ms, yielding near-instantaneous screen transitions. Incident photos opened in 320–700 ms, with p95 up to 1.8 s, which remains acceptable for verification because notifications are displayed first. Drop-frame rates were low across all tiers, and notification delivery was confirmed on Android 11–14. These results confirm stable client performance across tiers. The largest variation appears in photo open time, yet values remain operationally acceptable for incident verification. Low drop frame rates support smooth screen transitions and consistent notification handling on Android 11–14.

Table 8. Android mobile client display metrics

Device tier	Android version	UI render p50 (ms)	UI render p95 (ms)	Photo open p50 (ms)	Photo open p95 (ms)	Drop frames (%)	Notification compatibility
Flagship (high-performance)	11–14	45	80	320	900	0.7	✓
Medium	11–14	65	120	480	1300	1.5	✓
Entry	11–14	95	180	700	1800	3.2	✓

4.6. Usability testing with temple security personnel

A small-scale usability test with eight temple security personnel (N=8) found that the notification flow was easy to follow. Median task time was 12.4 seconds and the 95th percentile was 25.8 seconds. The task success rate reached 96.7 percent, and the system usability Scale score was 78.5, which is above the common 68 threshold and indicates good initial acceptability. Participants typically opened notifications and incident photos quickly. Slowdowns appeared during congested cellular periods, and the few failures occurred when photos had not fully downloaded on entry devices. Qualitative feedback highlighted two improvements: provide a clearer network status indicator and increase the contrast of the verify button to speed decisions in the field. Overall, the notification flow is straightforward and well accepted by early users. Implementing the network indicator and verify-button contrast changes is expected to reduce task times under variable network conditions without altering the system architecture.

5. CONCLUSION

The comparative analysis indicates that CLAHE is the most effective for improving image quality, achieving the lowest MSE of 21.16 and the highest PSNR of 38.13 dB. In contrast, HE and AHE, despite achieving higher detection accuracies of 83.33% and 80.21%, respectively, introduce noticeable distortion as reflected in their higher MSE values of 12,249.74 and 35,127.59. ROC analysis further clarifies this trade off. The best configuration, VGG-19 with HE, reached an AUC of 0.90±0.02 across five runs, indicating strong discriminative performance even when visual fidelity metrics are weaker. Complementary usability testing with temple security personnel reported a median task time of 12.4 seconds, a p95 of 25.8 seconds, a task success rate of 96.7%, and a system usability scale score of 78.5, suggesting that the system is operable and well accepted in field conditions. These results highlight that superior image quality, as indicated by MSE and PSNR, does not always correlate with superior object detection performance. Therefore, enhancement choices should be tuned to the end task, prioritizing AUC, F1-score, and operational recall when surveillance effectiveness is the primary objective. In practice, CLAHE is recommended when human interpretability and archival clarity are paramount, whereas HE may be preferable when maximizing automated detection under latency and resource constraints. Taken together, the ROC–AUC benchmarks and usability evidence provide actionable guidance for selecting enhancement–detector pairings to strengthen pratima protection in low-light conditions.

FUNDING INFORMATION

This research was funded by Lembaga Penelitian dan Pengabdian kepada Masyarakat (LPPM) Universitas Udayana through the Hibah Penelitian Unggulan Udayana under the Research Assignment Agreement No. B/255.235/UN14.4.A/PT.01.03/2024. The research was funded with a grant amounting to fifty-nine million rupiah, which greatly contributed to the successful completion of this study.

AUTHOR CONTRIBUTIONS STATEMENT

This journal uses the Contributor Roles Taxonomy (CRediT) to recognize individual author contributions, reduce authorship disputes, and facilitate collaboration.

Name of Author	C	M	So	Va	Fo	I	R	D	O	E	Vi	Su	P	Fu
Made Sudarma	✓	✓		✓		✓	✓	✓	✓	✓		✓		✓
Ni Wayan Sri Ariyani	✓	✓		✓	✓		✓	✓	✓	✓			✓	
I Putu Agus Eka Darma Udayana	✓	✓	✓	✓	✓	✓	✓	✓	✓	✓	✓			
Ida Bagus Gde Pranatayana				✓	✓	✓	✓		✓		✓			
Lie Jasa		✓		✓	✓		✓		✓					

C : **C**onceptualization
M : **M**ethodology
So : **So**ftware
Va : **Va**lidation
Fo : **Fo**rmal analysis
I : **I**nvestigation
R : **R**esources
D : **D**ata Curation
O : Writing - **O**riginal Draft
E : Writing - Review & **E**diting
Vi : **Vi**sualization
Su : **Su**pervision
P : **P**roject administration
Fu : **Fu**nding acquisition

CONFLICT OF INTEREST STATEMENT

The authors declare that they have no known competing financial interests or personal relationships that could have appeared to influence the work reported in this paper. The authors state no conflict of interest.

INFORMED CONSENT

Informed consent was not required for this study because the images used do not reveal identifiable personal information, and additional data were obtained from publicly available datasets.

ETHICAL APPROVAL

This study does not involve direct participation of human subjects or animals. The images used do not contain identifiable personal information and were obtained from publicly available datasets and derived data. Therefore, ethical approval was not required for this research.

DATA AVAILABILITY

Derived data supporting the findings of this study are available from the corresponding author [IPAEDU] upon reasonable request. Additional training and evaluation data were obtained from the publicly available in Kaggle at https://www.kaggle.com/datasets/washingtongold/exdark-dataset.

REFERENCES

[1] I. W. Mulyawan, I. M. S. Paramarta, and I. N. Suparwa, "Language contestation at Batukau Temple, Bali (a linguistic landscape study)," *Cogent Arts & Humanities*, vol. 9, no. 1, 2022, doi: 10.1080/23311983.2022.2090651.
[2] I. W. A. Ariawan and I. Irwansyah, "Criminal law policy against 'Pratima' theft: perspective of Balinese customary criminal law," *Scholars International Journal of Law, Crime and Justice*, vol. 7, no. 10, pp. 415–419, 2024, doi: 10.36348/sijlcj.2024.v07i10.001.
[3] C. Wei, W. Wang, W. Yang, and J. Liu, "Deep retinex decomposition for low-light enhancement," *arXiv:1808.04560*, 2018.
[4] C. Guo *et al*., "Zero-reference deep curve estimation for low-light image enhancement," *2020 IEEE/CVF Conference on Computer Vision and Pattern Recognition (CVPR),* Seattle, USA, 2020, pp. 1777-1786, doi: 10.1109/CVPR42600.2020.00185.
[5] Y. Jiang *et al.*, "EnlightenGAN: deep light enhancement without paired supervision," *IEEE Transactions on Image Processing*, 2021, pp. 2340-2349, doi: 10.1109/TIP.2021.3051462.
[6] W. Wu, J. Weng, P. Zhang, X. Wang, W. Yang, and J. Jiang, "URetinex-Net: retinex-based deep unfolding network for low-light image enhancement," in *2022 IEEE/CVF Conference on Computer Vision and Pattern Recognition (CVPR),* New Orleans, USA, 2022, pp. 5891-5900, doi: 10.1109/CVPR52688.2022.00581.
[7] Y. Wang and Z. Zhang, "Global attention retinex network for low light image enhancement," *Journal of Visual Communication and Image Representation*, vol. 92, Apr. 2023, doi: 10.1016/j.jvcir.2023.103795.
[8] W. Sultani, C. Chen, and M. Shah, "Real-world anomaly detection in surveillance videos," *2018 IEEE/CVF Conference on Computer Vision and Pattern Recognition,* Salt Lake City, USA, 2018, pp. 6479-6488, doi: 10.1109/CVPR.2018.00678.
[9] S. Reid, S. Coleman, P. Vance, D. Kerr, and S. O'Neill, "Using social signals to predict shoplifting: a transparent approach to a sensitive activity analysis problem," *Sensors*, vol. 21, no. 20, Oct. 2021, doi: 10.3390/s21206812.
[10] I. Muneer, M. Saddique, Z. Habib, and H. G. Mohamed, "Shoplifting detection using hybrid neural network CNN-BiLSMT and development of benchmark dataset," *Applied Sciences*, vol. 13, no. 14, Jul. 2023, doi: 10.3390/app13148341.
[11] S. Gangwar, R. Devi, and N. A. M. Isa, "Optimized exposer region-based modified adaptive histogram equalization method for contrast enhancement in CXR imaging," *Scientific Reports*, vol. 15, no. 1, Dec. 2025, doi: 10.1038/s41598-025-90876-6.
[12] M. Jourlin, "Image enhancement thanks to negative grey levels in the logarithmic image processing framework," *Sensors*, vol. 24, no. 15, Aug. 2024, doi: 10.3390/s24154969.
[13] F. Parera, N. Pinyol, and E. Alonso, "Image-based measurements of degree of saturation," in *E3S Web of Conferences: 4th European Conference on Unsaturated Soils (E-UNSAT 2020)*, Oct. 2020, pp. 1-4, doi: 10.1051/e3sconf/202019503010.
[14] B. Ye, S. Jin, B. Li, S. Yan, and D. Zhang, "Dual histogram equalization algorithm based on adaptive image correction," *Applied Sciences*, vol. 13, no. 19, Oct. 2023, doi: 10.3390/app131910649.
[15] Y. Y. Bae, D. J. Cho, and K. H. Jung, "A new log-transform histogram equalization technique for deep learning-based document forgery detection," *Symmetry*, vol. 17, no. 3, Mar. 2025, doi: 10.3390/sym17030395.
[16] J. Xiong *et al.*, "Application of histogram equalization for image enhancement in corrosion areas," *Shock and Vibration*, vol. 2021, no. 1, 2021, doi: 10.1155/2021/8883571.
[17] J. S. Cardenas *et al.*, "Image-based detection and classification of malaria parasites and leukocytes with quality assessment of Romanowsky-stained blood smears," *Sensors*, vol. 25, no. 2, Jan. 2025, doi: 10.3390/s25020390.

[18] P. Härtinger and C. Steger, "Adaptive histogram equalization in constant time," *Journal of Real-Time Image Processing*, vol. 21, no. 3, May 2024, doi: 10.1007/s11554-024-01465-1.
[19] R. C. Chen, C. Dewi, Y. C. Zhuang, and J. K. Chen, "Contrast limited adaptive histogram equalization for recognizing road marking at night based on YOLO models," *IEEE Access*, vol. 11, pp. 92926–92942, Aug. 2023, doi: 10.1109/ACCESS.2023.3309410.
[20] T. Xu, N. T. Umpon, and S. Auephanwiriyakul, "Staining-independent malaria parasite detection and life stage classification in blood smear images," *Applied Sciences*, vol. 14, no. 18, Sep. 2024, doi: 10.3390/app14188402.
[21] S. Soni, P. Singh, and A. A. Waoo, "Review of gamma correction techniques in digital imaging," *ShodhKosh: Journal of Visual and Performing Arts*, vol. 5, no. 5, May 2024, doi: 10.29121/shodhkosh.v5.i5.2024.1902.
[22] Y. Wang, Z. Liu, J. Liu, S. Xu, and S. Liu, "Low-light image enhancement with illumination-aware gamma correction and complete image modelling network," *2023 IEEE/CVF International Conference on Computer Vision (ICCV),* Paris, France, 2023, pp. 13082-13091, doi: 10.1109/ICCV51070.2023.01207.
[23] N. P. Sutramiani, N. Suciati, and D. Siahaan, "MAT-AGCA: multi augmentation technique on small dataset for Balinese character recognition using convolutional neural network," *ICT Express*, vol. 7, no. 4, pp. 521–529, Dec. 2021, doi: 10.1016/j.icte.2021.04.005.
[24] M. Xu, S. Yoon, A. Fuentes, and D. S. Park, "A comprehensive survey of image augmentation techniques for deep learning," *Pattern Recognition*, vol. 137, May 2023, doi: 10.1016/j.patcog.2023.109347.
[25] K. Alomar, H. I. Aysel, and X. Cai, "Data augmentation in classification and segmentation: a survey and new strategies," *Journal of Imaging*, vol. 9, no. 2, Feb. 2023, doi: 10.3390/jimaging9020046.
[26] K. Fukushima, "Artificial vision by deep CNN neocognitron," *IEEE Transactions on Systems, Man, and Cybernetics: Systems*, vol. 51, no. 1, pp. 76–90, 2021, doi: 10.1109/TSMC.2020.3042785.
[27] C. Tian, Y. Xu, Z. Li, W. Zuo, L. Fei, and H. Liu, "Attention-guided CNN for image denoising," *Neural Networks*, vol. 124, pp. 117–129, 2020, doi: 10.1016/j.neunet.2019.12.024.
[28] Z. J. Wang *et al.*, "CNN explainer: learning convolutional neural networks with interactive visualization," *IEEE Transactions on Visualization and Computer Graphics*, vol. 27, no. 2, pp. 1396–1406, Feb. 2021, doi: 10.1109/TVCG.2020.3030418.
[29] M. Krichen, "Convolutional neural networks: a survey," *Computers*, vol. 12, no. 8, Aug. 2023, doi: 10.3390/computers12080151.
[30] A. Zafar *et al.*, "Convolutional neural networks: a comprehensive evaluation and benchmarking of pooling layer variants," *Symmetry*, vol. 16, no. 11, Nov. 2024, doi: 10.3390/sym16111516.
[31] X. Zhao, L. Wang, Y. Zhang, X. Han, M. Deveci, and M. Parmar, "A review of convolutional neural networks in computer vision," *Artificial Intelligence Review*, vol. 57, no. 4, Apr. 2024, doi: 10.1007/s10462-024-10721-6.
[32] C. Zhou, Y. Liu, X. An, X. Xu, and H. Wang, "Optimization of deep learning architecture based on multi-path convolutional neural network algorithm," *Scientific Reports*, vol. 15, no. 1, Dec. 2025, doi: 10.1038/s41598-025-03765-3.
[33] A. Ponraj *et al.*, "A multi-patch-based deep learning model with VGG19 for breast cancer classifications in the pathology images," *Digital Health*, vol. 11, Jan. 2025, doi: 10.1177/20552076241313161.
[34] B. Kaushik, A. Chadha, and R. Sharma, "Performance evaluation of learning models for the prognosis of COVID-19," *New Generation Computing*, vol. 41, no. 3, pp. 533–551, Sep. 2023, doi: 10.1007/s00354-023-00220-7.
[35] J. Hossain, M. T. Islam, and M. T. H. K. Tusar, "Streamlining brain tumor classification with custom transfer learning in MRI images," in *2023 IEEE International Conference on Smart Information Systems and Technologies (SIST),* Astana, Kazakhstan, 2023, pp. 522-526, doi: 10.1109/SIST58284.2023.10223507.
[36] A. Breger *et al.*, "A study of why we need to reassess full reference image quality assessment with medical images," *Journal of Imaging Informatics in Medicine*, vol. 38, pp. 3444-3469, 2025, doi: 10.1007/s10278-025-01462-1.
[37] R. Gunawan, Y. Tran, J. Zheng, H. Nguyen, and R. Chai, "Optimizing natural image quality evaluators for quality measurement in CT scan denoising," *Computers*, vol. 14, no. 1, Jan. 2025, doi: 10.3390/computers14010018.
[38] A. W. Talab, N. K. Younis, and M. R. Ahmed, "Analysis equalization images contrast enhancement and performance measurement," *OAlib*, vol. 11, no. 4, pp. 1–11, 2024, doi: 10.4236/oalib.1111388.
[39] K. Hassanzadeh, S. A. Kandjani, R. Kheradmand, and S. A. Mortazavi, "Improving PSNR and computational efficiency in orthogonal ghost imaging," *Scientific Reports*, vol. 15, no. 1, Dec. 2025, doi: 10.1038/s41598-025-01283-w.
[40] C. Miller, T. Portlock, D. M. Nyaga, and J. M. O'Sullivan, "A review of model evaluation metrics for machine learning in genetics and genomics," *Frontiers in Bioinformatics*, 2024, doi: 10.3389/fbinf.2024.1457619.
[41] Z. Jingchun, G. E. Su, and M. S. Sunar, "Low-light image enhancement: a comprehensive review on methods, datasets and evaluation metrics," *Journal of King Saud University-Computer and Information Sciences*, vol. 36, no. 10, Dec. 2024, doi: 10.1016/j.jksuci.2024.102234.

BIOGRAPHIES OF AUTHORS

Made Sudarma holds a Doctorate from Udayana University, Indonesia, in 2012. He also holds an M.A.Sc. (Master of Applied Science) from SITE-OU: School of Information Technology and Engineering, Ottawa University, Canada in 2000. During his studies at SITE-OU, he was an assistant professor and a member of the research team of the built-in self-testing compaction generator field VLSI technology. He is also a professor of information technology science at the Electrical Engineering Study Program, Faculty of Engineering, Udayana University since 2019. His research includes internet and web applications, cloud computing, artificial intelligence, data warehousing and data mining, computer graphics, and virtual reality, as the author of books and as a reviewer in international and national journals. In addition, he also completed vocational education (IPU., ASEAN.Eng.) and is active in academic activities, and he also work as an information technology consultant in local government, private sector, and tourism. He can be contacted at email: msudarma@unud.ac.id.

Ni Wayan Sri Ariyani is a lecturer in the Industrial Engineering Study Program, Faculty of Engineering, Udayana University. She completed undergraduate studies at the Institute of Technology Sepuluh Nopember (ITS) Surabaya in 1992 in the field of Electronics Studies. The masters/masters program in 2009 at the Faculty of Economics and Business, Udayana University in the field of Marketing Management. The doctoral/S3 program was completed at the Udayana University Postgraduate Program in 2015 in the field of Marketing Management. Also active in the field of e-Procurement, e-Catalog and e-Purcashing implementation consultant as well as information technology and smart city planning consultant in several city/district governments in Bali and Nusa Tenggara. She has completed several studies, published several books, and is currently conducting a lot of research in the fields of technopreneurship, business incubators, digital business, and marketplaces. She can be contacted at email: sriariyani@unud.ac.id.

I Putu Agus Eka Darma Udayana completed his doctoral degree in Computer Science at Udayana University, Bali, Indonesia, in 2024, and earned his Master of Technology in Informatics Engineering from the Faculty of Engineering, Udayana University, in 2014. A certified engineer in Information Technology, he currently serves as the head of the Research Department at the Indonesian Institute of Business and Technology. His research interests encompass information systems, artificial intelligence, and image processing. Actively engaged in international conferences and as a member of several associations related to AI and image processing, he consistently contributes to advancing these fields. He is also involved in research and government projects focused ofn AI implementation and works as an information technology consultant for local governments, private organizations, and the tourism sector. He can be contacted at email: agus.ekadarma@gmail.com.

Ida Bagus Gde Pranatayana is a faculty member in the Agroecotechnology Study Program, Faculty of Agriculture, Udayana University, Indonesia. He earned his bachelor's degree in Plant Pests and Diseases from Udayana University in 2014. He further pursued his academic journey, obtaining a master's degree in Agricultural Biotechnology from the same institution in 2016. His research focuses on advancing agricultural practices, particularly in the development and application of biopesticide products for cocoa cultivation and the evaluation of pesticide products through data analysis methodologies. In addition to his research contributions, he has authored several publications, including e-books, that aim to enhance knowledge dissemination in the agricultural field. He can be contacted at email: pranatayana@unud.ac.id.

Lie Jasa is a lecturer in the Electrical Engineering Study Program, Faculty of Engineering, Udayana University, Denpasar, Bali. He completed his doctoral education in the field of Renewable Energy at the Institut Teknologi Sepuluh Nopember (ITS), Surabaya, in 2015 with a BPPS-Dikti scholarship. During his doctoral program, he also participated in a three-month sandwich program at Hiroshima University, Japan, in 2013. As a lecturer and researcher, his main research areas include renewable energy, electronic and information systems, VLSI technology, and artificial intelligence. Additionally, he is actively involved in writing and reviewing for national and international journals. He also has professional experience as a technology consultant in the fields of energy and electronic systems. He can be contacted at email: liejasa@unud.ac.id